PCCP

Accepted Manuscript

ROYAL SOCIETY OF CHEMISTRY

www.rsc.org/pccp

Statistical Modeling of the Reactions $Fe^+ + N_2O \rightarrow FeO^+ + N_2$ and $FeO^+ + CO \rightarrow Fe^+ + CO_2$

Vladimir G. Ushakov,[a,b] Jürgen Troe,[*,a,c,d] Ryan S. Johnson,[e] Hua Guo,[e] Shaun G. Ard,[f] Joshua J Melko,[f,g] Nicholas S. Shuman,[f] and Albert A. Viggiano[e,f]

March 2015

to be published in Phys. Chem. Chem. Phys.

---

[a]Max-Planck-Institut für Biophysikalische Chemie, Am Fassberg 11, D-37077 Göttingen, Germany

[b]Institute of Problems of Chemical Physics, Russian Academy of Sciences, 142432 Chernogolovka, Russia

[c]Institut für Physikalische Chemie, Universität Göttingen, Tammannstrasse 6, D-37077 Göttingen, Germany

[d]Laser-Laboratorium Göttingen, Hans-Adolf-Krebs-Weg 1, D-37077 Göttingen, Germany

[e]Department of Chemistry and Chemical Biology, University of New Mexico, Albuquerque, New Mexico 87131, USA

[f]Air Force Research Laboratory, Space Vehicle Directorate, Kirtland AFB, NM 87117-5776, USA

[g]Department of Chemistry, University of North Florida, Jacksonville, Florida 32224, USA

[*]Email: shoff@gwdg.de

Abstract

The rates of the reactions $Fe^+ + N_2O \rightarrow FeO^+ + N_2$ and $FeO^+ + CO \rightarrow Fe^+ + CO_2$ are modeled by statistical rate theory accounting for energy- and angular momentum-specific rate constants for formation of the primary and secondary cationic adducts and their backward and forward reactions. The reactions are both suggested to proceed on sextet and quartet potential energy surfaces with efficient, but probably not complete, equilibration by spin-inversion of the populations of the sextet and quartet adducts. The influence of spin-inversion on the overall reaction rate is investigated. The differences of the two reaction rates mostly are due to different numbers of entrance states (atom + linear rotor or linear rotor + linear rotor, respectively). The reaction $Fe^+ + N_2O$ was studied either with $^6Fe^+$ or with $^4Fe^+$ reactants. Differences in the rate constants of $^6Fe^+$ and $^4Fe^+$ reacting with N_2O are attributed to different contributions from electronically excited potential energy surfaces, such as they originate from the open-electronic shell reactants.

1. Introduction

The reaction $CO + N_2O \rightarrow CO_2 + N_2$ can be catalyzed by Fe^+ cations in the sequence of reactions

(1) $Fe^+ + N_2O \rightarrow FeO^+ + N_2$

(2) $FeO^+ + CO \rightarrow Fe^+ + CO_2$

whose rates have been measured in numerous studies.[1-7] The two reactions were found to have quite different rate constants at room temperature, $k_1(300\ K) = 3.2 \times 10^{-11}$ cm^3 molecule^{-1} s^{-1} and $k_2(300\ K) = 3.1 \times 10^{-10}$ cm^3 molecule^{-1} s^{-1}, and have markedly different temperature dependences.[7] A first attempt from our group to rationalize the observations[7] invoked the well-known two-state reactivity concept[8,9] with contributions from sextet and quartet pathways to reaction (1) while it assumed the dominance of a sextet contribution to reaction (2). The modeling was done with a statistical rate theory accounting for energy E- and angular momentum J-specific rate constants for formation and forward-reaction as well as backward-dissociation of the primary Fe^+N_2O and FeO^+CO adducts. In addition, it employed energetics determined by quantum-chemical calculations. The failure of this approach in ref. 7 tentatively was attributed to nonstatistical intrinsic dynamics of the adducts. A simple parametrization of this effect with a single fit parameter allowed one to mimic the experimental rate constants in a reasonable manner. Nevertheless, the question remained whether this interpretation is unique.

After completion of our work on reactions (1) and (2), an alternative analysis of rate constants for similar ion-molecule reactions was developed and applied to the reactions[10]

(3) $FeO^+ + CH_4 \rightarrow Fe^+ + CH_3OH$

$\rightarrow FeOH^+ + CH_3$

and[11]

(4) $FeO^+ + H_2 \rightarrow Fe^+ + H_2O$

$\rightarrow FeOH^+ + H$

It was confirmed that "rotational channel switching" was important, i.e. that different J-dependences of the energies of the loose entrance ($E_{0a}(J)$) and rigid exit ($E_{0b}(J)$) transition states into and out of the primary adducts (with $E_{0a}(J) > E_{0b}(J)$ at small J and $E_{0a}(J) < E_{0b}(J)$ at large J) had to be accounted for. In addition, an upper limit J_{max} for J was introduced which restricted the importance of primary adduct formation and back-dissociation. This "restricted" statistical model, employing two fit parameters (the quartet barrier E_{0b} for forward reaction of the adduct and J_{max}), turned out to be successful in reproducing not only absolute values of the rate constants, but temperature and isotope dependences over a broad range of energies as well. The fitted quartet transition state energy of reaction (4) was even found very close to a high-level quantum-chemical determination.[12] The success of the statistical model employed in refs. 10 and 11 prompted us to revisit reactions (1) and (2). In the present article, we analyze reaction (1) and (2) using the newer methods to see if the earlier fitting of the experiments with a single parameter representing "nonstatistical dynamics" could be replaced.

2. Modeling rate constants for the reaction $Fe^+ + N_2O \rightarrow FeO^+ + N_2$ (1)

We started with refined quantum-chemical calculations for reaction (1) such as described in Appendix A. Fig. 1 shows the new potential energy diagram of reaction (1) which supersedes the diagram shown in ref. 7. The vibrational frequencies and rotational constants of the reactants, the adducts, and the sextet and quartet transition states (TS) in the present modeling have been taken unchanged from the calculations, while the usually less precise energies of the barriers were used as fit parameters. We here refrain from more advanced quantum-chemical calulations for several reasons. Besides the barrier heights, other details of the potential energy surface are of relevance, such as the anisotropy of the Fe^+ - N_2O short-range potential which contributes to the parameter J_{max} in a complicated way (see below), the magnitude of spin–orbit coupling and the geometry of the crossing between sextet and quartet potential energy surfaces which determine the extent of sextet–quartet equilibration, and finally the possible contribution of electronically excited states which arise from the open–electronic shell reactants. The details of these features in the kinetics are lost such that the invested effort would appear wasteful. In addition, the extraction of the corresponding parameters from the kinetic data is not unique such that a qualitative agreement of fitted parameters with quantum–chemical values at best can be taken as an internal consistency test.

Details of our statistical modeling have been described in refs. 10 and 11 and are not repeated here. Instead, only the results are discussed. First, in the most simple models I and II, we assume a sufficiently long lifetime of the initial addition complex INT1 formed from Fe^+ and N_2O, such that sextet and quartet rovibrational states of INT1 can equilibrate. With this assumption we calculate the rate constant k_1 as a function of temperature (we note that the Langevin capture rate constant $k_{Langevin} \approx 8 \times 10^{-10}$ cm^3 molecule^{-1} s^{-1} is much larger than the experimental k_1). Assuming complete sextet-quartet equilibration in these models, the

strength of spin-orbit coupling does not further enter the calculated values of k_1. Models with incomplete equilibration and varying contributions from electronically excited states are considered afterwards.

Model I:

Assuming a very high TS energy in the sextet, in this model the reaction would be governed by the quartet barrier only. The comparison of the modeled k_1 with the experiments then leads to a fitted ^{4}TS energy of -433 cm^{-1} relative to the reactants (omitting the factor hc, all energies in this article are given in cm^{-1}) and $J_{max} = 47$. Fig. 2 shows (black line) fair agreement between modeling and experiment, however, without reproducing the experimentally observed marked change of the temperature coefficient near 300 K.

Model II:

Next, a lower ^{6}TS energy is assumed such that fluxes over ^{4}TS and ^{6}TS both contribute to the rate. In this case, the best fitting to the experiments is obtained with E(^{4}TS) = - 464 cm^{-1}, E(^{6}TS) = + 609 cm^{-1}, and $J_{max} = 45$, see Fig. 2 (red line). Again fair agreement is found. There is not, however, a major improvement with respect to the observed marked change of the temperature coefficient near 300 K. The dependence of the fitting on the parameter J_{max} is shown in Fig. 2 by a dashed blue line indicating the results for $J_{max} = \infty$, demonstrating a marked sensitivity to J_{max} (this applies to both of the models I and II).

Before proceeding to more sophisticated models, a few details of our approach should be explained. First, our fitting compares the measurements with the modeled rate constants,

optimizing the model parameters by a minimum least-squares procedure. Second, while the meaning of the transition state energies is clear, the meaning of J_{max} is not. On the one hand, J in reality cannot go to infinity, because then the well of the primary adduct INT1 would disappear and long-range capture into INT1 would cease to contribute to the rate. On the other hand, the restriction of J by J_{max} in our approach mimics "rigidity effects" in the capture (and the reverse dissociation). In the modeling we characterize the capture rate in terms of phase space theory for an isotropic ion-induced dipole potential.[13] However, during the ion-neutral approach, anisotropies of the potential generated by valence (or ion-permanent dipole) forces reduce the capture rate and introduce "rigidity" (for E- and J-dependent rigidity factors $f_{rigid}(E,J)$, see e.g. refs. 14 and 15). We assume that this effect is qualitatively accounted for by the restriction $J < J_{max}$. We finally note that the modeled TS energies of Fig. 2 are considerably different from the quantum-chemical calculations which gave $E(^4TS) = -2334$ cm^{-1} and $E(^6TS) = -401$ cm^{-1}, see Appendix A. Since the described quantum-chemical DFT calculations of the energies of ^4TS and ^6TS remain relatively uncertain[12] and several fit parameters are employed, one cannot prefer model II over model I. One can, however, investigate whether the representation of the experiments is improved by consideration of additional factors possibly also influencing the rates. This will be done in models III and IV described later in this text. A comment on the strong dependence of the modeling results on the parameter J_{max} in Fig. 2 should be made. It was shown in ref. 10 for the reaction $FeO^+ + CH_4$ (3) that the rate constant at large translational temperatures stops decreasing and finally increases with temperature. This increase is stronger for larger J_{max}, and the effect sets in near 3000 K. A similar phenomenon is observed in Fig. 2 at much smaller temperatures. We attribute this earlier onset to the fact that the reaction of N_2O with an atomic species like Fe^+ has a much smaller number of rotational entrance states than the reaction with a linear species like FeO^+. This is accounted for in the statistical modeling. When other processes like spin-inversion enter the overall rate, this phenomenon becomes less important, see below. The

much stronger decrease of the rate constant of reaction (1) with temperature in comparison to reactions (2) – (4), however, survives and can be attributed to the difference of reactions with atomic vs. linear reactants.

Model III:

Models I and II assumed sufficiently long lifetimes of the primary adducts INT1 such that complete equilibration of sextet and quartet states could be achieved. Before we discuss this assumption below, we investigate the consequences of incomplete equilibration. We do this by introducing an additional spin-inversion step into the kinetic scheme which may or may not influence the overall rate. In Models I and II, the sequence

(5) $Fe^+ + N_2O \Leftrightarrow$ INT 1 $\rightarrow$TS $\rightarrow$ products

was treated. Instead, we now consider the full mechanism

(6) $^6Fe^+ + N_2O \Leftrightarrow {}^6INT1 \rightarrow {}^6TS \rightarrow$ products

$^6Fe^+ + N_2O \Leftrightarrow {}^6INT1 \Leftrightarrow {}^4INT1 \rightarrow {}^4TS \rightarrow$ products

$^4Fe^+ + N_2O \Leftrightarrow {}^4INT1 \rightarrow {}^4TS \rightarrow$ products

$^4Fe^+ + N_2O \Leftrightarrow {}^4INT1 \Leftrightarrow {}^6INT1 \rightarrow {}^6TS \rightarrow$ products

The rate of the spin-inversions $^6INT1 \rightarrow {}^4INT1$ and $^4INT1 \rightarrow {}^6INT1$ in the language of statistical rate theory is expressed by $W_{SQ}/h\rho_6$ and $W_{SQ}/h\rho_4$, respectively, where ρ_6 and ρ_4 are the vibrational densities of states of INT1 in the sextet and quartet and W_{SQ} are effective

numbers of activated complex states for spin-inversion. The W_{SQ}, such as given by numbers of states at the sextet-quartet crossing seam multiplied by spin-inversion probabilities, are treated as additional parameters. It may seem non-intuitive that we treat W_{SQ} as an energy independent fitting parameter, as the included spin-inversion probability certainly depends on energy in a Landau-Zener type way. Equally important in determining the spin inversion probability, however, are details of the multidimensional crossing of the sextet and quartet potentials. As these details are not available at this time, detailed theoretical treatment of W_{SQ} in this system is premature, and thus is treated as an effective fit parameter.

Appendix B descibes modeling details of the kinetic scheme of reaction (6), including the given spin-inversion steps. Fig. 3 illustrates the results (black line). With the parameters $E(^4TS) = -700\ cm^{-1}$, $E(^6TS) = +244\ cm^{-1}$, $J_{max} = 59$ and $W_{SQ} = 829$, the fitted black line reproduces the marked change of the temperature coefficient of the rate constant much better than models I and II. We tested the significance of the parameter J_{max} and Fig. 3 includes the results (dashed black line). With the parameters $E(^4TS) = -387\ cm^{-1}$, $E(^6TS) = +1044\ cm^{-1}$, $J_{max} = \infty$ and $W_{SQ} = 1286$, the fitted line also reproduces the experiments acceptably. Unfortunately the non-uniqueness of the modeling at this stage still prevents us from choosing one model over the other. We note that the introduction of incomplete equilibration even brought the nonstatistical model of ref. 7 into fairly good agreement with the experimental temperature dependence. In this situation one cannot judge the significance of the fitted individual parameters, because changes in one can be compensated by changes in other parameters. However, their importance in statistical modeling illustrates places where further refinements may be necessary. Meanwhile, a way out of the dilemma has been provided by the new experiments presented in ref. 16. This has led to the formulation of the extended model IV.

Model IV:

In a separate study[16] we measured the rate of reaction (1) replacing $^6Fe^+$ by electronically excited $^4Fe^+$. Varying the fit parameters of model III, in any case one predicts a larger rate constant, $k(^4Fe^+)$, such as e.g. shown by the black line in comparison to the red line in Fig.4 for the sextet rate constant, $k(^6Fe^+)$ (both lines calculated with the fit parameters of the black line in Fig. 3). In contrast to this, the experimental rate constant for $^4Fe^+$ was found to be $k(^4Fe^+) = 2.3x10^{-11}$ cm^3 molecule^{-1} s^{-1} at 300 K, i.e. being significantly smaller than $k(^6Fe^+)$.[16] We emphasize that this observation could in no way be reproduced by parameter variation in models I - III. This forced us to further refine model III by taking into account the open-electronic shell character of the Fe^+ cations.

There are 7 potential energy surfaces originating from the 28 fine-structure states of $Fe^+(^4F)$ while 5 potential energy surfaces start from the 30 states of $Fe^+(^6D)$. In the present work we neglect fine-structure splittings of the Fe^+ states, but we include electronic partition functions for the 7 quartet and 5 sextet potentials of the forming adducts. (The individual fine-structure splittings will be accounted for in ref. 16.) We first arbitrarily assume that only 1 out of the 7 quartet potentials starting from $Fe^+(^4F)$ leads to the bound adduct INT1 while only a single out of the 5 sextet potentials starting from $Fe^+(^6D)$ contributes to the reaction. In this case, with the fit parameters $E(^4TS)$= -1260 cm^{-1}, $E(^6TS)$= -130 cm^{-1}, J_{max}= 232, and W_{SQ}=868, the experimental $k(^6Fe^+)$ is well reproduced (magenta line in Fig.4), while $k(^4Fe^+)$ still is much larger (yellow line in Fig.4). Next, we assume that not only attractive potentials may lead from $^6Fe^+$ into INT1, but repulsive potentials may also get there after crossing the attractive quartet potential. This crossing may or may not involve additional energy barriers

such that the fitted ^{6}TS barrier would correspond to an average barrier height being higher than that of the lowest sextet potential. Again fitting the modeled sextet rate constants to the experiments, with five sextet and one quartet potential and the fit parameters E(^{4}TS) = -2214 cm^{-1}, E(^{6}TS) = +218 cm^{-1}, J_{max} = 59, and W_{SQ} = 3059, the experimental k($^6Fe^+$) is well reproduced (dashed green line in Fig.4). On the other hand , k($^4Fe^+$) drops to the blue line in Fig.4, giving a value not much larger than the experimental value at 300 K. Finally, increasing W_{SQ} to infinity such that spin-conversion completely equilibrates ^{4}INT1 and ^{6}INT1, with five sextet and one quartet potential and the fit parameters E(^{4}TS)=-740 cm^{-1}, E(^{6}TS)=+587 cm^{-1}, and J_{max}=58, again the experimental sextet rate constants are well reproduced (green line in Fig.4), while the quartet rate constant further drops to the brown line in Fig.4, giving about one half the experimental value at 300 K. This could be compensated by assuming that more than a single potential originating from $^4Fe^+$ contributes to the reaction. Clearly we cannot conclude on more details of the contribution of excited excited electronic states to the overall reaction. Nevertheless it appears certain that only a minor fraction of the states originating from $^4Fe^+$ contribute significantly while a major fraction of the states originating from $^6Fe^+$ does. More details of the modeling of the quartet rate constant are given in ref. 16. Here we conclude that model IV is able to reproduce the available rate constants for both the reactions of $^4Fe^+$ and $^6Fe^+$ with N_2O remarkably well.

Below we further discuss the role of spin-inversion in these reactions. We treat the models with the rate constants in Fig. 4 as limiting cases, because they embrace the experimental quartet rate constants within the estimated experimental uncertainties.[16] The fitted values for E(^{4}TS) are in qualitative agreement with the quantum-chemical values of Appendix A, values for E(^{6}TS) being somewhat higher than the quantum-chemical calculations, which may be due to the averaging over barriers from several sextet states, and values for W_{SQ} which correspond to only partial equilibration of sextet and quartet adducts such that spin-inversion rates enter into the overall rate constant.

3. Average adduct lifetimes

In this section we come back to the question whether the rate of spin-inversion enters the rate of the overall process or is fast enough to allow for a complete equilibration of sextet and quartet INT1. Model IV is the only model that has been found to fit the data for both the $^4Fe^+$ and $^6Fe^+$ states reacting with N_2O. However, both partial and complete equilibration of sextet and quartet adducts INT1 fit the data within this model. We further approach this aspect of the reaction by calculating average decay rate constants of INT1 employing the statistical models after their fitting to the rate measurements. Since the specific rate constants $k(E,J) = W(E,J)/h\rho(E,J)$ for forward- and backward-dissociation of INT1 depend on the density of states $\rho(E,J)$ of INT1, the well depth of INT1 is of relevance. We estimate $\rho(E,J)$ with the parameters from the DFT calculations given in Appendix A. At steady-state, capture into the adduct and forward- plus backward-reaction fluxes are equal. The concentration of adducts at an angular momentum J and in the energy intervall (E,E+dE) is given as dC. One then has

$$(7)\quad k_{cap}dE = (2J+1)W_A(E,J)\exp(-E/k_BT)\,dE/hQ$$

$$= [W_A(E,J) + W_{TS}(E,J)]\,dC/h\rho(E,J)$$

and, hence, the total concentration of adducts is given by

$$(8)\quad C=\frac{1}{Q}\int\sum(2J+1)\,\rho(E,J)\exp(-E/k_BT)\left\{W_A(E,J)/\left[W_A(E,J)+W_{TS}(E,J)\right]\right\}dE$$

(Q denotes products of partition functions canceling later on; W_A is the number of open rovibrational channel states in the entrance leading into the adduct ; W_{TS} is the number of states at the transition state between adduct and products). The average decay rate constant <k> of the adducts finally follows as

$$(9)\quad \langle k\rangle=\frac{1}{C}\int\frac{W_A+W_{TS}}{h\rho}\,dC$$
$$=\frac{1}{h}\frac{\int\sum(2J+1)\,W_A\exp(-E/k_BT)\,dE}{\int\sum(2J+1)\exp(-E/k_BT)\left\{W_A/\left[W_A+W_{TS}\right]\right\}\rho(E,J)\,dE}$$

The average lifetime τ is expressed through $\tau = 1/\langle k\rangle$. One obtains results such as shown in Fig. 5. The figure includes lines for a model with full sextet-quartet equilibration (black line) in INT1 and a model without any spin-inversion (red line). The fact that the lines are close to each other is accidental and due to the fact that the two cases involve individual fittings to the experiments (for the fitting parameters , see the caption of Fig. 5). What is relevant, however, is the observation that <k> in the shown temperature range is at least 20 times smaller than the smallest adduct vibrational frequency ((3-5) x 10^{12} s^{-1}, see Appendix A). It is, therefore, plausable that spin-inversion at least partly equilibrates sextet and quartet adducts INT1. Our calculations with model IV are compatible with this conclusion. It should be noted that <k> for this system is similar to those calculated for reactions 3 and 4[10,11] where full equilibration between sextet and quartet aducts was found to model the data well. A more detailed discussion of spin-inversion rates will be given in ref. 16.

4. Modeling rate constants for the reaction $FeO^+ + CO \rightarrow Fe^+ + CO_2$ (2)

In ref. 7 we modeled the experimental rate constants of reaction (2) without spin-inversion on a single sextet potential surface. Again we attributed the difference between statistical modeling and experiment to nonstatistical dynamics, employing a similar parameter for the latter as for reaction (1). Based on our experience with the restricted statistical modeling used in Sections 2 and 3, we now also apply the latter to reaction (2). Before doing this, we extend our quantum-chemical calculations to include potentials originating from quartet FeO^+. Fig. 6 shows the derived energy diagram. Details of the corresponding molecular parameters are given in Appendix A. The calculated diagram suggests a possibility for a contribution from a low quartet TS pathway after sextet-quartet spin-inversion has taken place.

Employing the rotational constants and vibrational frequencies from our present calculations (see Appendix A), but leaving the TS energies and J_{max} as adjustable parameters, we proceed as described for models I and II in section 2. (We note that the Langevin rate constant for reaction (2) similar to reaction (1) amounts to about 7 x10 $^{-10}$ cm^3 $molecule^{-1}$ s^{-1} .) First assuming reaction with a single TS only, one can well reproduce the measurements with the fitted parameters E(TS) = -6471 cm^{-1} and J_{max} = 74. Fig. 7 illustrates the results. However, the fitted barrier of E(TS) is much smaller than the calculated sextet barrier E(^{6}TS) of -1387 cm^{-1}. This supports the assumption of a dominant pathway involving spin-inversion, as the calculated energy of the quartet barrier is equal to -6602 cm^{-1}. Next, we again inspect the possibility of two pathways, one governed by the ^{4}TS and one by the ^{6}TS. The fit to the experiments with this approach leads to E(^{6}TS) = -2116 cm^{-1}, E(^{4}TS) = -10108 cm^{-1} and J_{max} = 73. If E(^{6}TS) is fixed at the calculated value -1387 cm^{-1} from Fig. 6, E(^{4}TS) = -10169 cm^{-1}

and J_{max} = 73 are obtained. Fig. 8 demonstrates that the two fits reproduce the measurements equally well and no advantage over Fig. 7 is obtained because the sextet channel makes only a minor contribution. We note that the fitted energy parameters again are in fair agreement with our quantum-chemical calculations, see Appendix A and Fig. 6. We finally calculate average lifetimes of the adduct INT1. If there were no spin-inversion, the fitted decay rate constant between 10^{10} and 10^{11} s^{-1} would correspond to many passages of the sextet-quartet crossing seam. As the best fitting of the experiments corresponds to a dominant pathway with low TS energy, complete equilibration between sextet and quartet states in INT1 corresponds to a larger decay rate constant of the adduct. Nevertheless, its average value around 10^{12} s^{-1} still corresponds to multiple passages of the crossing during the lifetime of INT1 such that spin-inversion should again be effective. Because we have no quartet rate measurement, we cannot establish whether spin-inversion partly or completely equilibrates sextet and quartet adducts INT1.

5. Discussion

One may ask why reactions (1) and (2) have so different properties, i.e. rate constants with markedly different absolute values and different types of temperature dependences. Although the present fitting of restricted statistical rate models to the experimental data is not unique, the present approach provides an internally consistent general picture. Reaction (2) is faster than reaction (1), first, because there is a quartet pathway with lower TS energy. The similarity between fitted and calculated TS energies confirms that the reactions both involve sextet-quartet spin-inversion, partly or completely equilibrating the states of INT1. Although the accuracy of our quantum-chemical calculations is limited and the fitting of the

experiments is not unique (and the employed rate theory is certainly oversimplified), there is little doubt about the marked participation of spin-inversion. The question, whether the rate of spin-inversion enters the overall rate constant or is so effective that sextet- and quartet adducts INT1 are fully equilibrated, is more difficult to answer. The marked change of the temperature coefficient of the rate of reaction (1) near room temperature in principle could be attributed to a contribution of spin-inversion to the overall rate . However, it could also be reproduced for reaction (1) by a model with equilibration of sextet and quartet adducts and the contribution of only a single potential out of the multitude of quartet potentials originating from the open-shell reactants. The measurement for the reaction of $^4Fe^+$ with N_2O clearly corresponds to the latter situation. One may ask whether a similar effect is not observed for reaction (2). The quartet pathway dominates over the sextet pathway in reaction (2) to a greater extent than for reaction (1). Therefore, different temperature dependences of the two pathways do not become noticeable in the overall rate. In addition, there are fewer electronically excited potentials starting from sextet and quartet FeO^+ .There is, however, another basic difference between reactions (1) and (2) – (4). The number of entrance states in reaction (1) corresponds to an atomic ion + linear neutral rotor situation while reactions (2) – (4) correspond to linear rotor + linear rotor (or symmetric top in reaction (3)) situations. That difference has severe consequences for the numbers of entrance states $W_A(E,J)$ in the two reactions. This is accounted for in statistical modeling: it causes a much earlier decrease followed by an earlier increase of the rate constants with increasing temperature for reaction (1) than for reactions (2) - (4).

6. Conclusions

After our success in modeling the reactions of FeO^+ with H_2 and CH_4 using restricted statistical modeling, we have revisited the modeling of the title reactions. Previously, we had introduced non-statistical terms which we show here are no longer necessary. For the reaction

of Fe^+ with N_2O, models where that the sextet and quartet rovibrational states of the entrance channel complex can equilibrate do not reproduce the temperature dependence of the rate constant for sextet reactant. Incorporating a spin-inversion step then allows for a fitting of the $^6Fe^+$ data. However, such models predict that $^4Fe^+$will react faster than that for $^4Fe^+$ in contradiction to the experimental results presented in ref. 16. The way out of that dilemma is to allow for only some of the fine-structure states to contribute to the reaction. The best fit is when a minority of the quartet surfaces contribute to the reaction, while a majority of the sextet surfaces play a role. Similarly, modeling the reaction of FeO^+ with CO can also be done with the restricted statistical modeling. Lifetime calculations show that spin-inversion is likely not complete.

Experiments of the described type unfortunately cannot fit the relevant molecular parameters in a unique way. They can only highlight which properties are of relevance and thus should be analyzed in more detail in future work. One is even unable to clearly distinguish between fully statistical and nonstatistical dynamics. However, our work shows that energy- and angular momentum-specific statistical rate theory , in connection with semi-quantitative quantum-chemical information, can account for the available experimental data and allows for an extrapolation into unexplored conditions

Acknowledgments

The authors would like to thank Peter Armentrout, Helmut Schwarz, Sason Shaik, and Jeremy Harvey for insightful conversations. This work is supported by the Department of Energy Office of Science, Office of Basic Energy Research (DE-FG02-05ER15694 to H.G.) and by the Air Force Office of Scientific Research (AFOSR-2303EP to A.A.V.). S.G.A.

acknowledges the support of Boston College Institute of Scientific Research. J.T. acknowledges support from the EOARD Grant-Award FA8655-11-13077.

References

1 M. M. Kappes and R. H. Staley, J. Am. Chem. Soc., 1981, **103**, 1286 – 1287.

2 V. Baranov, G. Javehery, A. C. Hopkins and D. K. Bohme, J. Am. Chem. Soc., 1995, **117**, 12801 – 12809.

3 V. Blagojevic, G. Orlova and D. K. Bohme, J. Am. Chem. Soc., 2005, **127**, 3545 – 3555.

4 V. V. Lavrov, V. Blagojevic, G. K. Koyanagi, G. Orlova and D. K. Bohme, J. Phys. Chem. A, 2004, **108**, 5610 – 5624.

5 P. B. Armentrout, L. F. Halle and J. L. Beauchamp, J. Chem. Phys., 1982, **76**, 2449 – 2457.

6 J. M. C. Plane and R. J. Rollafson, J. Chem. Soc. Faraday Trans., 1996, **92**, 4371 – 4376.

7 J. J. Melko, S. G. Ard, J. A. Fournier, J. Li, N. S. Shuman, H. Guo, J. Troe and A. A. Viggiano, Phys. Chem. Chem. Phys., 2013, **15**, 11257 -11267.

8 D. Schröder, S. Shaik and H. Schwarz, Acc. Chem. Res., 2000, **33**, 139 – 145.

9 D. K. Böhme and H. Schwarz, Angew. Chem. Int. Ed., 2005, **44**, 2336 -2354.

10 S. G. Ard, J. J. Melko, V. G. Ushakov, R. Johnson, J. A. Fournier, N. S. Shuman, H. Guo, J. Troe and A. A. Viggiano, J. Phys. Chem. A, 2014, **118**, 2029 – 2039.

11 S. G. Ard, J. J. Melko, O. Martinez, V. G. Ushakov, A. Li, R., S. Johnson, N. S. Shuman, H. Guo, J. Troe and A. A. Viggiano, J. Phys. Chem. A, 2014, **118**, 6789 – 6797.

12 A. Altun, J. Breidung, F. Neese and W. Thiel, J. Chem. Theory Comput., 2014, **10**, 3807 – 3828.

13 A. I. Maergoiz, E. E. Nikitin, J. Troe and V. G. Ushakov, J. Chem. Phys., 2002, **117**, 4201-4213.

14 J. Troe, V. G. Ushakov and A. A. Viggiano, J. Phys. Chem. A, 2006, **10**, 1491 – 1499.

15 J. Troe and V. G. Ushakov, J. Phys. Chem. A, 2006, **110**, 6732 – 6741.

16 S. G. Ard, R. S. Johnson, J. J. Melko, O. Martinez jr, N. S. Shuman, V. G. Ushakov, H. Guo, J. Troe and A. A. Viggiano, Phys. Chem. Chem. Phys. (subsequent article).

17 S. Grimme, J. Antony, S. Ehrlich and H. Krieg, J. Chem. Phys., 2010, **132,** 154104.

18 E. R. Johnson and A. D. Becke, J. Chem. Phys., 2006, **124**, 174104.

19 F.Weigend and R. Ahlrichs, Phys. Chem. Chem. Phys., 2005, **7**, 3297-3305.

20 F. Neese, F. Wennmohs, A. Hansen and U. Becker, Chem. Phys. 2009, **356**, 98-109.

21 F. Neese, Wiley Interdisc. Rev.- Comput. Mol. Sci., 2011, **2**, 73-78.

Appendix A Molecular parameters

A1: Quantum-chemical calculations

The stationary points of the sextet and quartet potential energy surfaces of reactions (1) and (2) were determined using density functional theory (DFT) at the B3LYP level. This functional has been found to give reasonable geometric parameters for reactions (3) and (4), see refs. 10 and 11. Furthermore, atom-pairwise dispersion corrections[17] were included using Becke-Johnson dampening.[18] Triple-zeta valence basis sets were augmented with 2d polarization functions and sp diffuse functions on N, O, and C atoms and 2f polarization and sppd polarization functions on the Fe atom.[19] Resolution of Identity (RI-J) and Chain of Spheres (COSX) approximations[20] were utilized with equivalent quality auxiliary basis sets. Vibrational frequencies were determined by the method of finite differences in which atoms are displaced by 0.005 a_0. Calculations were carried out using the ORCA 3.0 electronic structure package.[21]

A2: Parameters for reactions (1) and (2)

Energies of stationary points, rotational constants, and vibrational frequencies (all in cm^{-1}) as calculated with the method from A1 (IS=reactants, FS=products, 6=sextet, 4=quartet).

$Fe^+ + N_2O \rightarrow FeO^+ + N_2$ (1) (see Fig.1)

Energies (including zeropoint energy contributions)

Sextet: 0.0(IS), -5932.5(INT1), -401.3(TS), -22075.7(INT2), -13587.1(FS)

Quartet: 860.3(IS) -8897.6(INT1), -2333.8(TS), -18864.0(INT2), -8837.0(FS)

Rotational constants

FeO^+(4): 0.559; FeO^+(6): 0.504; N_2 : 2.02; N_2O: 0.423; INT1(4): 0.0654, 0.0677, 2.07;

INT1(6): 0.0610, 0.0627, 2.07; TS(4): 0.0674, 0.0687, 3.28; TS(6): 0.0811, 0.0897, 0.815;

INT2(4): 0.0937, 0.110, 0.641; INT2(6): 0.0747, 0.0747, 94.5

Vibrational frequencies

FeO^+(4): 974.7; FeO^+(6): 836.4; N_2: 2448.0; N_2O: 605.5,1315.0, 2317.7; INT1(4): 111.0, 264.2, 542.9, 568.1, 1228.5, 2363.4; INT1(6): 105.6, 239.2, 534.8, 547.3, 1215.1, 2357.9;

TS(4): -849.2, 118.6, 132.1, 284.1, 583.1, 2179.1; TS(6): -578.6, 56.5, 212.3, 435.2, 538.5, 1967.6; INT2(4): 177.9, 249.8, 283.3, 341.5, 917.4, 2443.4; INT2(6): 120.3, 215.7, 231.7, 270.5, 822.2, 2451.1

$FeO^+ + CO \rightarrow Fe^+ + CO_2$ (2) (see Fig.6)

Energies (including zeropoint energy contributions)

Sextet: 0.0(IS), -11426.1(INT1), -1387.0(TS), -22361.6(INT2), -16599.5(FS)

Quartet: 4750.1(IS), -9822.6(INT1), -6602.1(TS), -16760.8(INT2), -15739.2(FS)

Rotational constants

CO: 1.94; CO_2: 0.391; INT1(4): 0.0961, 0.116, 0.552; INT1(6): 0.0694, 0.0694, 818; TS(4): 0.105, 0.127, 0.603; TS(6): 0.0917, 0.106, 0.686; INT2(4): 0.0567, 0.0567, 1760; INT2(6): 0.0534, 0.0534, 40.4

Vibrational frequencies

CO: 2201.4; CO_2: 679.7, 1362.1, 2387.8; INT1(4): 210.5, 325.0, 360.1, 402.3, 1003.0, 2297.8; INT1(6): 173.3, 273.3, 277.8, 309.7, 796.8, 2314.5; TS(4): -474.4, 322.8, 363.9, 421.4, 826.2, 2178.2; TS(6): -574.7, 174.1, 241.7, 358.8, 719.0, 2115.2; INT2(4): 111.3, 240.9, 631.6, 644.8, 1383.2, 2441.0; INT2(6): 31.9, 208.8, 631.5, 646.9, 1360.5, 2418.3

Appendix B Statistical modeling including finite spin-inversion rates

Assuming that spin-inversion equilibrates sextet and quartet adducts, the overall rate constant of the reaction is given by

$$(a1) \quad k=\frac{k_B T}{hQ}\int\sum_J (2J+1)\exp(-E/k_B T)W_A\left[W_{TS}/(W_A+W_{TS})\right]dE/k_B T$$

where $W_{TS} = W_{TS}(4) + W_{TS}(6)$ is the number of states of the quartet and sextet transition states, $W_A = W_A(4) + W_A(6)$ is the number of quartet and sextet reactant entrance states, and Q is the relevant product of partition functions. For $W_{TS} \gg W_A$, the expression [ ] in eq. (*a*1) goes to unity and k approaches the capture rate constant, here given by the Langevin rate constant.

The expression [ ] in eq. (a1) corresponds to the fraction of adducts reacting by forward-flux from the adduct over the TS to products and it is obtained from the simple kinetic scheme operating for equilibrated sextet and quartet adducts. When the full scheme of eq. (6) is treated, the spin-inversion rate constants k_6 and k_4, as represented and given below eq.(6), also enter the rate constant k. The product W_A[ ] in eq. (*a*1) then is replaced by an expression G(E,J) given by

$$(a2) \quad G(E,J)=\frac{W_{SQ}W_A+W_A(4)\{W_A(6)+W_{TS}(6)\}}{W_{SQ}(W_A+W_{TS})+\{W_A(4)+W_{TS}(4)\}\{W_A(6)+W_{TS}(6)\}}W_{TS}(4)+$$
$$+\frac{W_{SQ}W_A+W_A(6)\{W_A(4)+W_{TS}(4)\}}{W_{SQ}(W_A+W_{TS})+\{W_A(4)+W_{TS}(4)\}\{W_A(6)+W_{TS}(6)\}}W_{TS}(6)$$

In the limit of $W_{SQ} \to \infty$, i.e. full equilibration of sextet and quartet adducts, eq. (*a*1) is obtained. When $W_{SQ} \to 0$, eqs.(*a*1) and (*a*2) reduce to two separate sextet and quartet rate constants. (It should be noted that the difference in partition functions of sextet and quartet reactants in eq. (*a*1) is neglected. Furthermore, in eq.(*a*2) W_{SQ} for simplicity is used as a constant fit parameter independent of E and J.)

Figure Captions

Fig. 1 Potential energy diagram of reaction (1) (red: quartet, black: sextet; numbers: energies/hc in cm^{-1}, including zeropoint energy contributions; results from quantum-chemical calculations of the present work, see Appendix A).

Fig. 2 Statistical modeling of the rate constant for reaction (1) (●: experimental data from ref. 7; black line: model I with a single quartet transition state only and fit parameters $E(^4TS) = -433\ cm^{-1}$ and $J_{max} = 47$, dashed blue line: as black line, but with $E(^4TS) = -199\ cm^{-1}$ and $J_{max}=\infty$; red line: model II with single quartet and sextet potentials and fit parameters $E(^4TS) = -464\ cm^{-1}$, $E(^6TS) = +609\ cm^{-1}$ and $J_{max} = 45$).

Fig. 3 As Fig. 2, but for model III, i.e. single quartet and sextet potentials with finite rate of sextet ⇔ quartet transitions (black line: fit parameters $E(^4TS) = -700\ cm^{-1}$, $E(^6TS) = +224\ cm^{-1}$, $W_{SQ} = 829$ and $J_{max} = 59$; dashed black line: fit parameters $E(^4TS) = -387\ cm^{-1}$, $E(^6TS) = +1044\ cm^{-1}$, $W_{SQ} = 1286$ and $J_{max} = \infty$).

Fig. 4 As Fig. 3, but for model IV, i.e. quartet and sextet potentials with finite rates of sextet ⇔ quartet transitions and variable numbers of reacting quartet and sextet states (red line: sextet and black line: quartet rate constants for single reacting quartet and sextet potentials without contribution of additional electronically excited potentials, modeling with the parameters of the black line from Fig. 3; magenta line: sextet and yellow line: quartet rate constants for single reacting quartet and sextet potentials out of 7 quartet and 5 sextet potentials, modeling with the parameters $E(^4TS) = -1260\ cm^{-1}$, $E(^6TS) = -130\ cm^{-1}$, $J_{max} = 232$ and $W_{SQ} = 868$; dashed green line: sextet and blue line: quartet rate constants for single contributing quartet and 5 contributing sextet

potentials out of 7 quartet and 5 sextet potentials, modeling with the parameters $E(^4TS)$=-2214 cm $^{-1}$, $E(^6TS)$= + 218 cm^{-1} , J_{max} = 59 and W_{SQ} =3059; green line: sextet and brown line: quartet rate constants for single contributing quartet and 5 contributing sextet out of 7 quartet and 5 sextet potentials, modeling with the parameters $E(^4TS)$=-740 cm $^{-1}$, $E(^6TS)$=+587 cm^{-1} , J_{max} =58 and W_{SQ} =∞; for more details, see the text) as well as the experimental data (open circles).

Fig. 5 Average decay rate constants of adducts INT1 (black curve: full equilibration of sextet and quartet adducts by efficient spin-inversion , model parameters corresponding to the black line in Fig. 3; red line: sextet adducts only, without spin-inversion i.e. W_{SQ} = 0, model parameters otherwise also corresponding to the black line in Fig.3).

Fig. 6 Potential energy diagram of reaction (2) (red: quartet, black: sextet, numbers = energies/hc in cm^{-1} including zeropoint energies; results from present work, see Appendix A).

Fig. 7 Statistical modeling of the rate constant for reaction (2) (●: experimental data from ref. 7; black line: modeling with sextet potential only and fit parameters E(TS) = -6483 cm^{-1} and J = 74).

Fig. 8 As Fig. 7, but with sextet and quartet potentials assuming full equilibration of sextet and quartet states of adduct INT1 (red line: fit parameters $E(^4TS)$ = -10108 cm^{-1}, $E(^6TS)$ = -2116 cm^{-1} and J_{max} = 73; dashed black line: fit parameters $E(^4TS)$ = -10169 cm^{-1}, $E(^6TS)$ = -1387 cm^{-1} and J_{max} = 73, $E(^6TS)$ here being fixed to the calculated value from Fig. 6).

Fig. 9 As Fig. 5, but for reaction (2) (calculations for the potential with fit parameters used for Fig. 8).

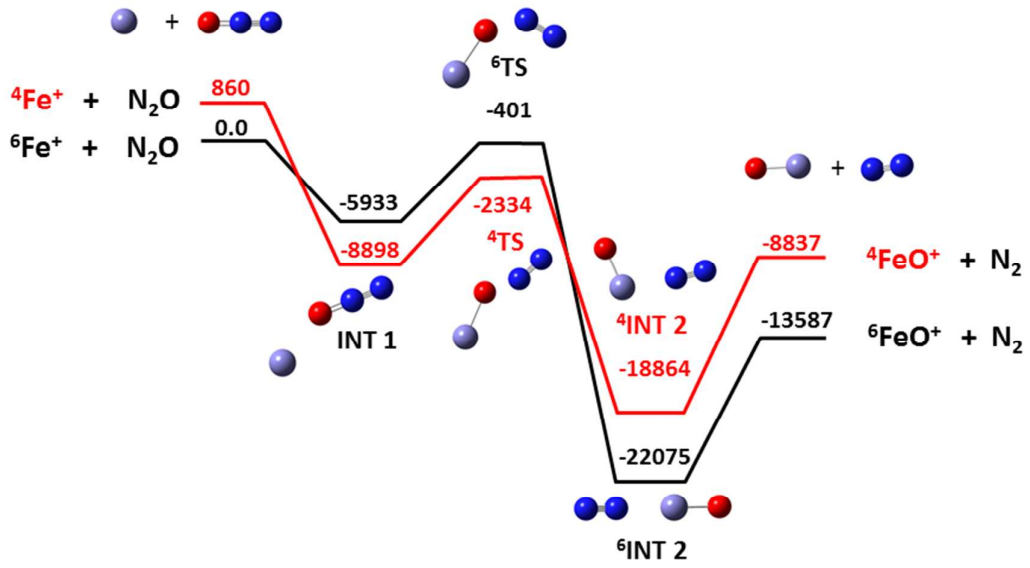

Fig 1

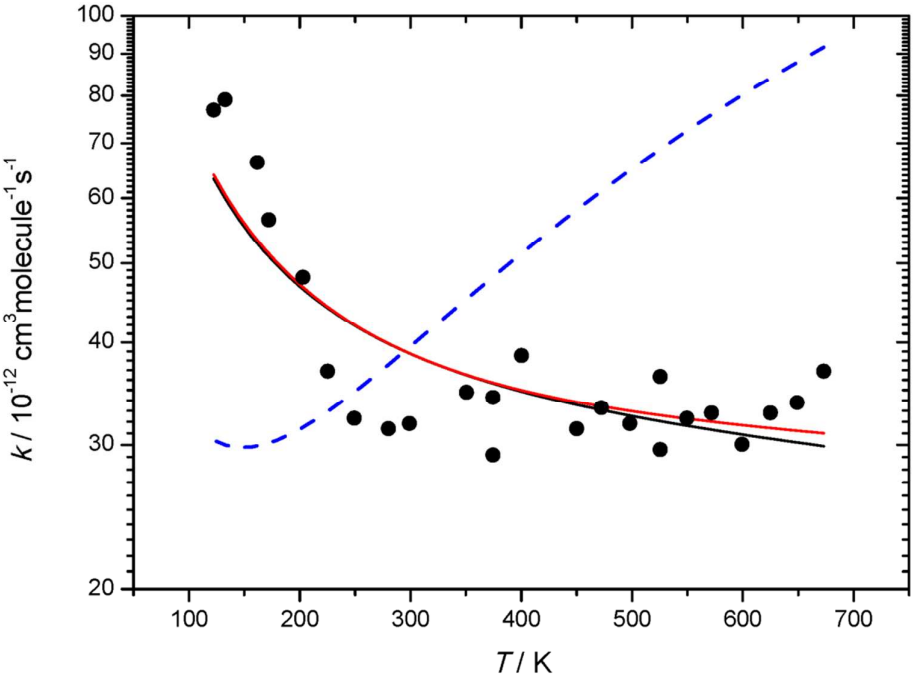

Fig. 2

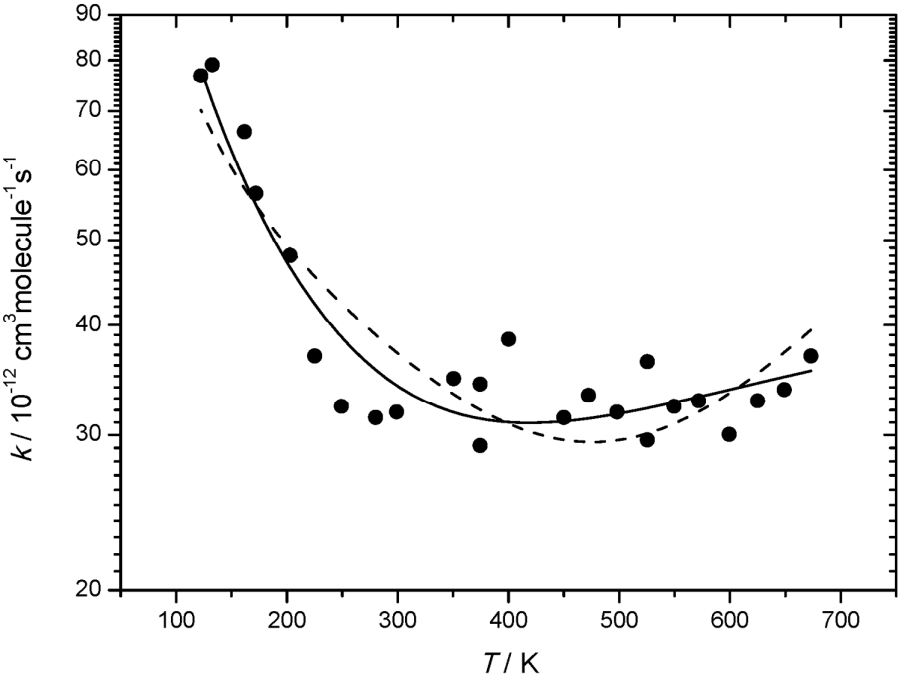

Fig. 3

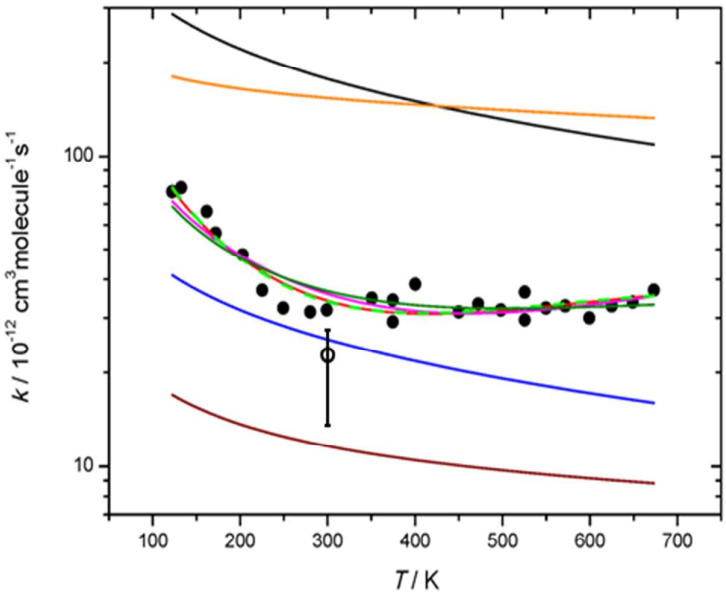

Fig. 4

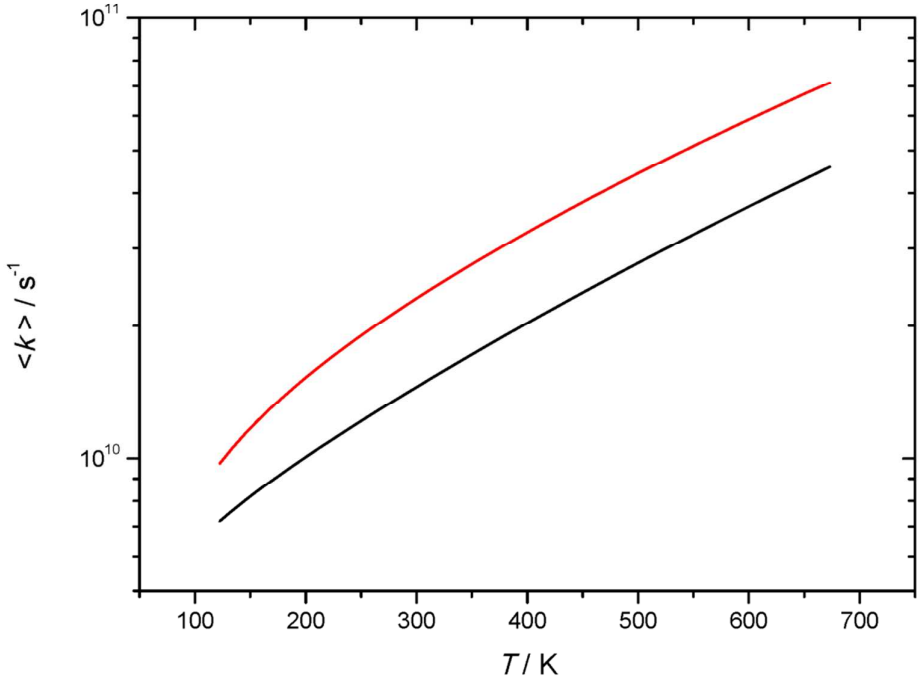

Fig. 5

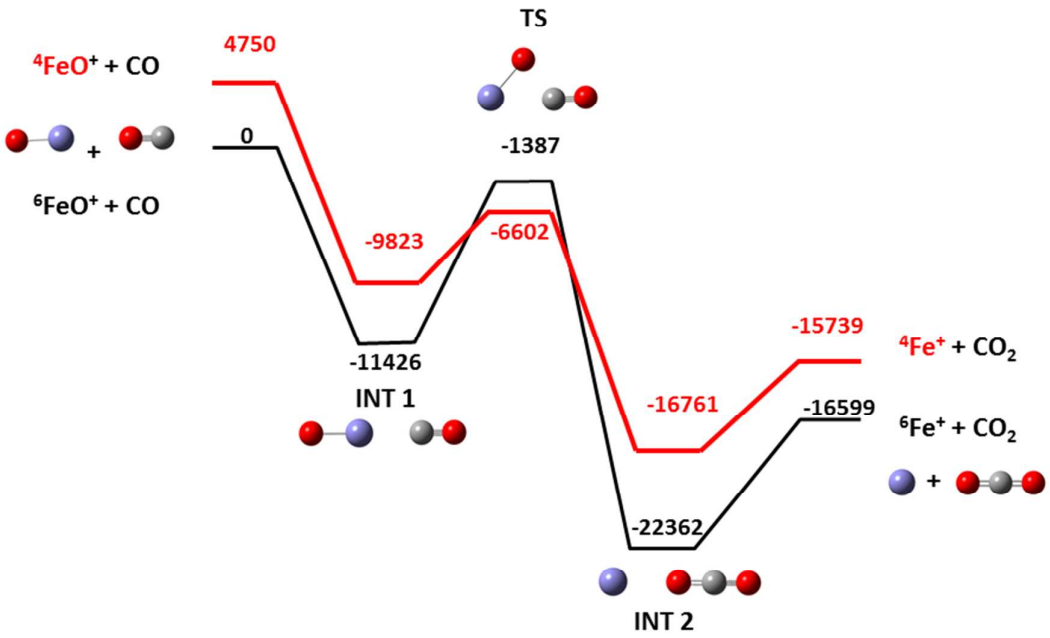

Fig 6

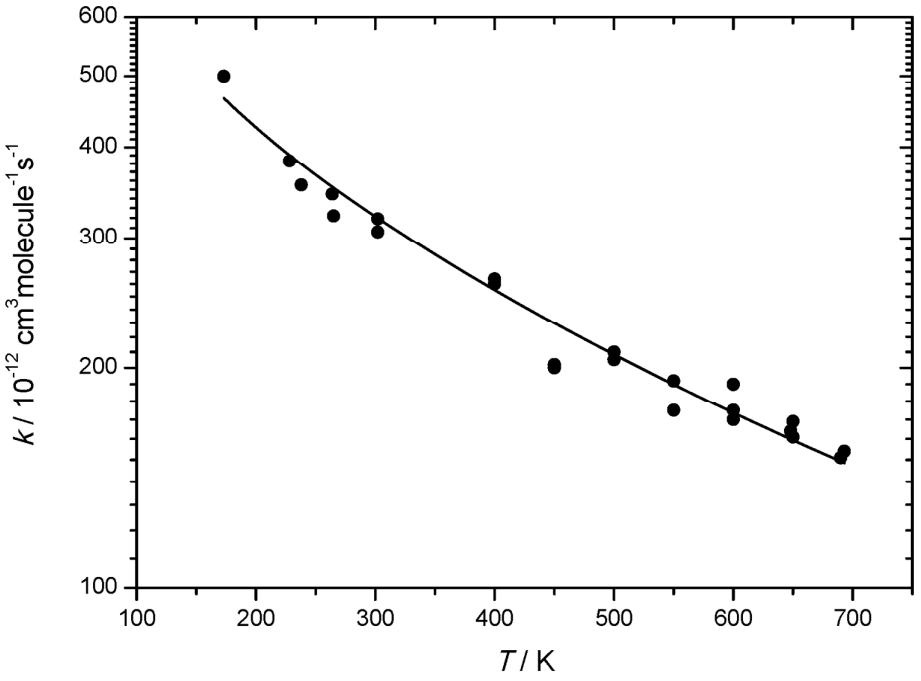

Fig. 7

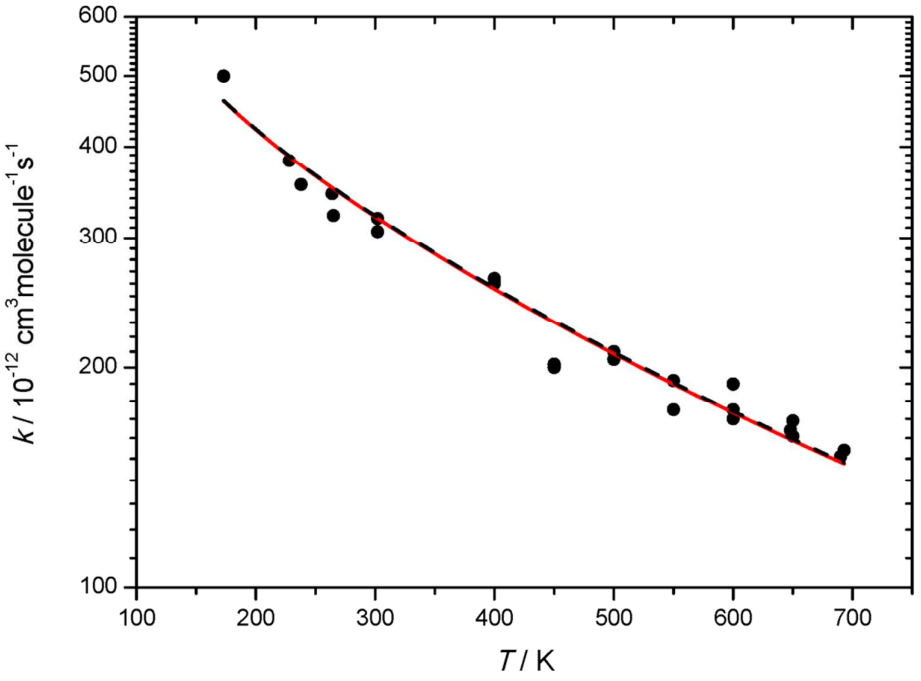

Fig. 8

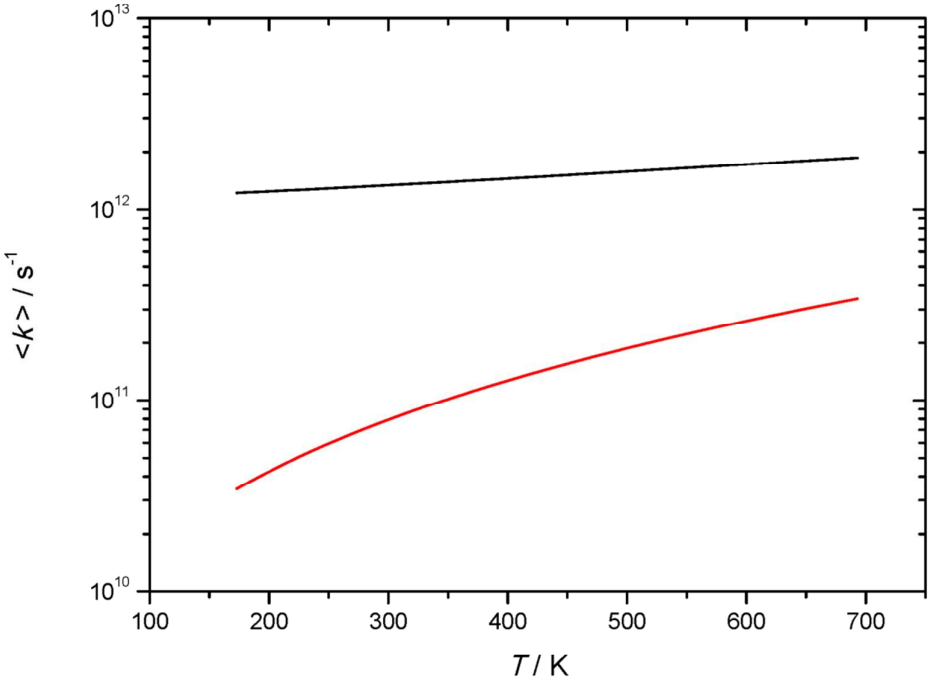

Fig. 9